Available online at www.sciencedirect.com

ScienceDirect

Ceramics International 40 (2014) 4445–4453

CERAMICS INTERNATIONAL

www.elsevier.com/locate/ceramint

Photoluminescence properties of praseodymium doped cerium oxide nanocrystals

A.C. Cabral[a], L.S. Cavalcante[b], R.C. Deus[c], E. Longo[d], A.Z. Simões[c,*], F. Moura[a]

[a]*Universidade Federal de Itajubá – Unifei – Campus Itabira, Rua São Paulo 377, Bairro Amazonas, P.O. Box 355, 35900-37, Itabira, Minas Gerais, Brazil*
[b]*CCN-DQ-GERATEC, Universidade Estadual do Piauí; João Cabral, N. 2231, P.O. Box 381, CEP: 64002-150, Teresina-PI, Brazil*
[c]*Universidade Estadual Paulista – Unesp – Faculdade de Engenharia de Guaratinguetá, Av. Dr Ariberto Pereira da Cunha 333, Bairro Pedregulho, P.O. Box 355, 12.516-410, Guaratinguetá, São Paulo, Brazil*
[d]*Laboratório Interdisciplinar em Cerâmica, Instituto de Química, Universidade Estadual Paulista, P.O. Box 355, 14801-907 Araraquara, São Paulo, Brazil*

Received 24 June 2013; received in revised form 27 August 2013; accepted 27 August 2013
Available online 21 September 2013

Abstract

The structure and photoluminescence (PL) properties of CeO_2 nanocrystals synthesized by the microwave-assisted hydrothermal (MAH) method with different praseodymium (Pr^{3+}) ions contents were performed. X-ray diffraction (XRD), transmission electron microscopy (TEM), diffuse reflectance ultraviolet-visible (UV-vis), Fourier transform Raman (FT-Raman) spectroscopies and PL measurements at room temperature were employed. XRD patterns indicated that the nanocrystals are free of secondary phases and crystallize in the cubic structure while FT-Raman revealed a typical scattering mode of fluorite type. The UV-vis spectra suggested the presence of intermediate energy levels in the band gap of these nanocrystals. The most intense PL emission was obtained for CeO_2 nanocrystals doped with 1.6% of Pr^{3+} ions and smaller particle size.

Keywords: A. Ceramics; B. Chemical syntheses; B. Powder metallurgy; C. X-ray diffraction

1. Introduction

Nanocrystalline CeO_2 powders have been considered as an important nanomaterial for applications in catalysts [1], fuel cells [2], ultraviolet absorbers [3], hydrogen storage materials [4], oxygen sensors [5], optical devices [6] and polishing materials [7]. Several methods have been developed to prepare ultrafine CeO_2 powder, including conventional hydrothermal [8], co-precipitation [9], polymeric precursor [10], flow method [11], organometallic decomposition [12], microwave-assisted heating [13] and microwave-hydrothermal [14–16] methods. Among the various methods, the hydrothermal crystallization is an interesting process to directly prepare pure fine oxide powders with reduced contamination and low synthesis temperature. However, conventional-hydrothermal method requires longer soaking times at a low temperature (below 200 °C) to obtain the ceria powders. For this reason, the introduction of microwave heating to the conventional-hydrothermal method is advantageous for the synthesis of various ceramic powders because microwave heating permits a reduction of processing time and energy cost. Likewise, particles with desired size and shape can be produced if parameters, such as: solution pH, reaction temperature, reaction time, solute concentration and the type of solvent are carefully monitored [17–22]. A modification of the hydrothermal method developed by Komarneni et al. [23–25] involves the introduction of microwaves during the hydrothermal synthesis to increase the kinetics of crystallization by one to two orders of magnitude compared to the conventional hydrothermal. The microwave-assisted hydrothermal (MAH) method shows advantages such as rapidity, convenience and cost-effectiveness. Ceria systems with nanosized particles were successfully synthesized by the MAH method utilizing a relatively low temperature and short reaction time [26]. Here, the authors describe the formation conditions of ceria via the MAH method reported in detail, and the advantages of microwave irradiation introduced.

As we know, there are few works describing MAH route for the synthesis of pure CeO_2 nanoparticles. Gao et al. [27] reported for the first time the preparation of ceria nanoparticles

*Corresponding author. Tel.: +551 231 232 765; fax: +551 231 232 800.
E-mail address: alezipo@yahoo.com (A.Z. Simões).

0272-8842/$ - see front matter
http://dx.doi.org/10.1016/j.ceramint.2013.08.117

(1.6 nm) and nanorods (20 nm) under microwave-assisted conditions. Corradi et al. [28] also reported the synthesis of cubic CeO_2 crystals (5.7 nm) under microwave-assisted hydrothermal route around 194 °C for only 5 min. No calcination process or surfactant was required. The MAH method is getting very attractive in all areas of synthetic chemistry because it can boost some advantages over other synthetic methods [24]. This method has been extensively used in organic synthesis [25–27] and more recently this technique has also been widely applied to prepare inorganic nanostructured materials, [28–31] with a wide range of applications [32–34]. In particular, Bilecka and Niederberger have reported the versatility of the method for the synthesis of nanoparticles, [35] while Baghbanzadeh et al. [36] have presented a complete review on the subject. da Silva et al. [42] prepared $SrTi_{1-x}Fe_xO_3$ nanocubes by means of a microwave-assisted hydrothermal (MAH) method at 140 °C. According to high-resolution transmission electron microscopy (HRTEM) results, these nanocubes are formed by a self-assembly process of small primary nanocrystals. In the another paper of the group [38], $BaZrO_3$ (BZO) nanoparticles were nucleated, grown and subsequently self-assembled into a 3D decaoctahedronal architecture via a microwave-assisted hydrothermal (MAH) method. A theoretical model, based on the presence of uncoordinated bonds and/or charge distribution in the distorted constituent octahedral $[ZrO_6]$ clusters and cuboctahedral $[BaO_{12}]$ clusters of the material, can be related to the change in both surface and internal defects during crystal growth. $BaZrO_3$ microcrystals were also obtained using the microwave assisted hydrothermal method (MAH) at 140 °C for 40 min [39]. The growth mechanism for the formation of $BaZrO_3$ with decaoctahedron-shape was analyzed in detail, and the nature of the mechanism follows a non-classical growth process involving mesoscale self-assemblies of nanoparticles. The PL emission is considered to be closely related to the crystal structure and their corresponding distorted metal-oxygen polyhedra. Among the properties of pure or doped cerium oxide nanoparticles, photoluminescence has been the object of several publications [40–49] but these may appear as not very conclusive as some experimental facts were not definitely explained. For example, even the attribution of the most intense peak at 400 nm to Ce_6O_{11} clusters firstly proposed by Morshed et al. [19], was considered a hypothetical by the authors themselves. Comparisons of results from different studies are complicated due to the fact that different syntheses produce particles with different surface or bulk defects, oxygen vacancies and ratio of reduced Ce^{3+}. The point is 4 or 5 bands may appear in a relatively narrow region around 400 nm and their respective attribution is not clear, to our knowledge. On this basis, systematic experiments may be useful to extract reliable information from photoluminescence spectra. Tok et al. [47] synthesized undoped and rare earth (RE) doped (RE=Pr, Gd, and Sm) ceria nanoparticles by hydrothermal synthesis method, achieving with weak agglomeration with the size range of 13–25 nm, by hydrothermal method using hexamethylenetetramine (HMT) as precipitating agent. They found that the crystallite size of RE doped decrease with the increase in RE content and the lattice parameter slightly increase with the increase in RE doping content. Rare earth doped ceria nanopowders were prepared by hydrothermal treatment at 100 °C for 2 h. In another work, Li et al. [48] have studied the formation of La or Pr-doped flower-like mesoporous ceria microspheres by a unique calcination of La or Pr-doped $Ce(OH)CO_3$ microspheres hydrothermally synthesized with the aid of glucose and acrylic acid. Prepared flower-like ceria-based materials have a novel hierarchical architecture with mesoporous structure and high surface area, which can obviously facilitate the catalytic combustion of methane, compared with general La or Pr-doped ceria. The presence of La or Pr can promote the production of oxygen vacancies and improve oxygen mobility, which result in enhancing the oxygen-storage capacity of the flower-like ceria and its catalytic performance for the methane combustion. To our knowledge, the formation of the ceria-praseodymium system with high surface area was mentioned in a few reports [48]. This is the reason why we decided to synthesize Ce–Pr nanoparticles focusing on links between the structure and the photoluminescent behavior of CeO_2 nanoparticles through a simple and fast microwave-assisted hydrothermal (MAH) method. Our work indicates that MAH is important not only for the use of a short treatment time and low temperature but also for the possibility to control the morphological and structural properties without the use of surfactants at low processing time. Compared to literature, similar type of defects were evidenced after introduction of Pr resulting in different PL behavior.

2. Experimental procedure

CeO_2 nanoparticles were synthesized by the MAH method. Cerium(IV) ammonium nitrate (5×10^{-3} mol L^{-1} $Ce(NH_4)_2(NO_3)_6$, 99.9% purity) was dissolved in 80 ml of deionized water under constant stirring for 15 min at room temperature. Pr_2O_3 (99.9% purity, Aldrich) was dissolved in nitric acid, and also added to the solution. Subsequently, 1 ml of 2 M KOH (p.a, Merck) was slowly added in the solution until the pH 10 was reached. The resulted solution was transferred into a sealed Teflon autoclave and placed in a hydrothermal microwave (2.45 GHz, maximum power of 800 W). The reactional system was heat treated at 100 °C for different soaking times (1, 2, 4 and 8 min) with a heating rate fixed at 10 °C/min. The pressure in the sealed autoclave was stabilized at 1.2 atm. The autoclave was cooled to the room temperature naturally. CeO_2 nanoparticles were collected and washed with acetone several times and then dried at 80 °C in an oven. The obtained nanocrystals were characterized by X-ray powder diffraction (XRD) using a (Rigaku-DMax/2500PC, Japan) with Cu-Kα radiation (λ=1.5406 Å) in the 2θ range from 20 to 75° with 0.2°/min. The crystallite size (d) of CeO_2 was calculated using Scherrer equation $d = k\lambda/\beta \cos\theta$, where k is constant, λ is wavelength of X-rays and β is the full width at half maximum (FWHM) for (111) reflection measured from slow scan where θ is the diffraction angle of the main peak. Raman spectra were collected (Bruker RFS-100/S Raman spectrometer with Fourier transform). A 1064 nm YAG laser was used as the excitation source, and its power was kept at 150 mW. The

morphology of as-prepared samples was observed using a CM200 transmission electron microscope (Philips, Netherlands) operated at 200 kV. PL measurements were taken at room temperature. Ultraviolet–visible (UV–vis) spectroscopy for the optical absorbance spectra of CeO_2 powders was taken using Cary 5G equipment. PL properties were measured with a Thermal Jarrel-Ash Monospec 27 monochromator and a Hamamatsu R446 photomultiplier. The excitation source was 350.7 nm wavelength of a krypton ion laser (Coherent Innova) keeping their power at 15 mW.

3. Results and discussion

The XRD patterns of as-prepared ceria nanoparticles showed the same crystalline structure for all the synthesis conditions used (Fig. 1a). All of the peaks can be well-indexed to a pure cubic structure of CeO_2 (space group: $Fm\bar{3}m$) with lattice constant $a=5.411$ Å, which is in good agreement with the JCPDS file for CeO_2 (JCPDS 34–394). It is worth noting that the overwhelmingly intensive diffraction peak is located at $2\theta=28.660^{\circ}$, which is from the [111] lattice plane of fcc CeO_2. No peak of any other phase was detected. The broadening of the peaks indicates that the crystallite sizes are small (4–9 nm), following the literature [49]. The average crystallite sizes calculated by Debye Scherrer is around 3.2; 2.9, 4.80 and 5.10 nm at a Pr contents of 0; 1.6; 5 and 10 mol%, respectively. It is obvious that the amount of rare-earth changes the CeO_2 crystal growth. As the average diffusion distance for the diffusing solute is short and the concentration gradient is steep in concentrated solutions, much diffusing material passes per unit time through an unit area. A clear evidence that CeO_2 is formed instead $Ce(OH)_x$ come from the fact that nitrate salts of ceria were preferably used since these salts were easily dissociable in few milliliters of water and the friable mass formed (Ce^{4+}) after treating with acid, reacted spontaneously with the mineralizer to produce a highly exothermic reaction. When cerium nitrate is used as the precursor salt and reacted with an acid to dissolve it, the Ce^{3+} ion is oxidized to Ce^{4+} ion and them acidic mass reacts exothermically with the mineralizer. It forms a by-product salt (KNO_3) that surrounds the hydroxide product. In the oxidizing atmosphere, dehydration occurs, converting the hydroxide intermediate to oxide. In the MAH methods, the conversion to oxide is more rapid due to the effect of energetic radiations assisting the transformation to CeO_2 instead $Ce(OH)_x$. Fig. 1b reveal the dependence of lattice parameter and unit cell volume as a function of praseodymium content. As the amount of Pr content is increased lattice parameters tend to decrease indicating that the rare-earth shortened the average distance for the diffusing solute. The XRD patterns of samples correspond to the same symmetry of fluorite-type cubic structure. A slight reduction of the lattice parameter with Pr^{3+} ions incorporation is in agreement with the results of Takasu et al. [50]. The slight variation observed is neverthel in all cases aress within the experimental uncertainty of the measurement. The lattice parameter values in the range of $a=5.41$ Å $\pm$ 0.005. High resolution or possibly neutron diffraction measurements would

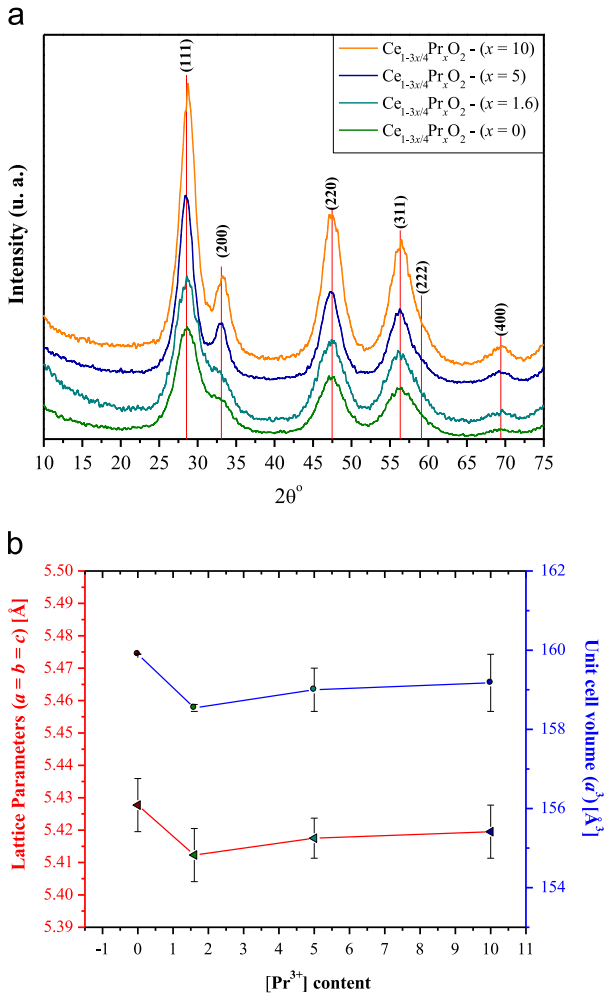

Fig. 1. (a) X-ray diffraction pattern of $Ce_{1-3/4x}Pr_xO_2$ nanoparticles synthesized at 100 °C in the MAH method under KOH mineralizer at different contents: (a) 0; (b) 1.6; (c) 5.0 and (d) 10. (b) Dependence of Pr content as a function of lattice parameter as unit cell volume.

be more efficient to evaluate the effect of Pr incorporation in the lattice cell parameter of the nanopowders, given the wide features of the XRD pattern and that the variation in the cubic cell parameter falls inside the range of experimental uncertainty of this study.

Fig. 2 confirm the formation of pure CeO_2 nanocrystals by FT-Raman spectrum. Cubic fluorite structure-metal dioxides have a single Raman mode at 464.5 cm^{-1}, which has F2 g symmetry and can be viewed as a symmetric breathing mode of the O atoms around each cation. Since only the O atoms move, the vibrational mode is nearly independent of the cation mass [51–52]. As shown, three additional low intensity second scattering Raman bands are detected around 266, 598 and 726 cm^{-1}, respectively. These bands are usually assigned to the presence of extrinsic oxygen vacancies generated into the ceria lattice improving diffusion rate of bulk oxygen after praseodymium addition. The fast structural organization of CeO_2 nanocrystals obtained by the MAH method can be related to heating process which occurs from the interior to the surface. The microwave energy is transformed into heat through the interaction

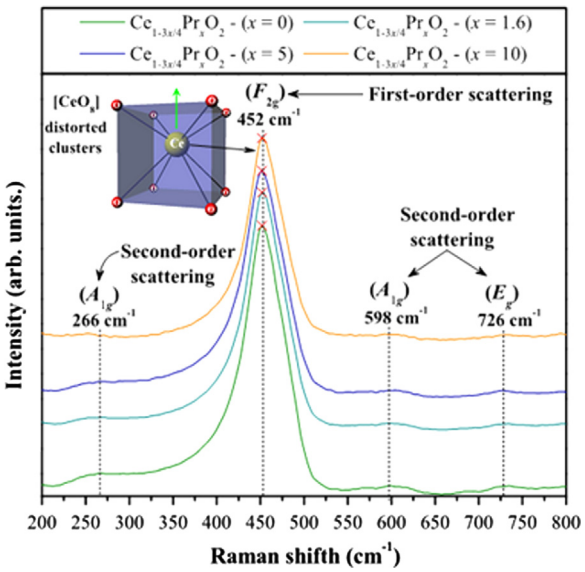

Fig. 2. Raman spectra of $Ce_{1-3/4x}Pr_xO_2$ nanoparticles synthesized at 100 °C in the MAH method under KOH mineralizer at different contents: (a) 0; (b) 1.6; (c) 5.0 and (d) 10.

between molecules and atoms with the electromagnetic field. This interaction results in an internal and volumetric heating of the powders which promotes the formation of temperature gradients and heat flows. It is well known that the Raman signal is affected by these randomly oriented vacancies that distort long range ordering. The defect formation is a known source of structural disorder, and thus breakdown of translational symmetry occurs, which results in relaxation of the $k \cong 0$ selection rule for Raman scattering and hence phonons from all parts of the Brillouin zone contribute to the spectra. Praseodymium oxide (Pr_2O_3), on the other hand, with Pr^{3+} ions in state of valence 3+, crystallize in the body-centered lattice and belong to the space group Ia3 (Th7). The unit cell contains the two primitive cells having eight formula units. Factor group analysis predicts a total of 22 Raman active modes distributed as 4Ag+4Eg+14Fg. The measured Raman spectra exhibit a characteristic strong feature at 452 cm^{-1}.The position of this Raman band is related to the strength of the RE–O bond and for Pr_2O_3, extrapolating from other RE Raman data, can be expected to be at ≈ 266, 598, 458 and 726 cm^{-1}.

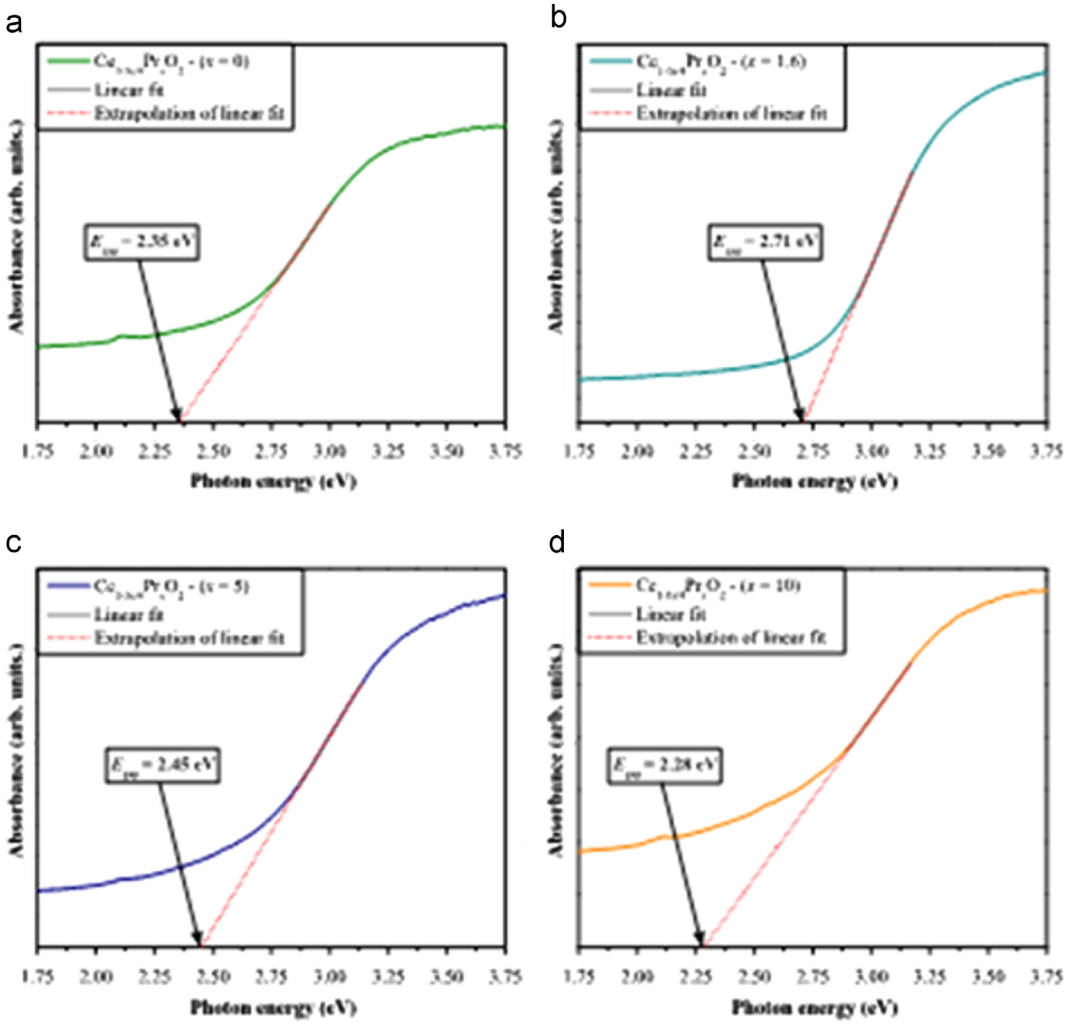

Fig. 3. UV–vis absorbance spectra of $Ce_{1-3/4x}Pr_xO_2$ nanoparticles synthesized at 100 °C in the MAH method under KOH mineralizer at different contents: (a) 0; (b) 1.6; (c) 5.0 and (d) 10.

Fig. 3 illustrates the UV–vis spectral dependence of absorbance for the ordered CeO_2 particles. The maximum absorption was located at around 400 nm with respective band gap values determined from the Kubelka-Munk model [53]. The optical energy band gap is related to the absorbance and to the photon energy by the following Eq. (1):

$$h\nu\alpha \propto (h\nu - E_g^{opt})^2 \quad (1)$$

where α is the absorbance, h is the Planck constant, ν is the frequency and E_g^{opt} is the optical band gap [54]. The band gap was deduced by fitting the absorption data to the direct transition equation by extrapolating of the linear portions of the curves to absorption equal to zero. In structurally ordered CeO_2 nanocrystals, the absorbance measurements suggest a non uniform band gap structure with a tail of localized states (see Fig. 4a–d). The main changes in the optical band gap [$E_{(gap)}$] energy can be correlated to the reduction of structural defects or localized states inside the band gap which decreases the intermediary energy levels due to the reduction of oxygen vacancies located at crystal structure. This behavior indicates that these samples present a certain structural order degree in agreement with the Raman spectra. The estimated band gaps were ranged between 2.65 to 2.97 eV. The uncertainty of these values was estimated at 0.05 eV. As Pr content increases, the optical band gap of the sample initially increases and then decreases because new levels of energy are formed promoting the appearance of intermediate electronic levels in the band gap. The irregularities in the optical band gap values can be related with the different preparation methods, shape, average crystal size and structural order–disorder degree in the lattice.

TEM images of CeO_2 nanocrystals obtained at different Pr contents are shown in Fig. 4. CeO_2 synthesized by MAH under KOH at 100 °C for 8 min, revealing the particle sizes are approximately range from 6 to 12 nm (Fig. 4a–d). The resultant particles have a spherical shape with approximately 6 nm in diameter. According to the image, most of the grains of CeO_2 nanoparticles are homogeneous with an average particle size of 6.7, 7.9, 8.8 and 11.5 nm as Pr content increases of 0, 1.6, 5 and 10, respectively. Undoped CeO_2 powders obtained displays poor contrast and intense agglomeration amongst extremely fine particles. The small size of the CeO_2 nanocrystals synthesized by MAH can be explained quite simply. It is postulated that at the start of the reaction a large number of nucleus forms in the solution and as the reaction takes place in a very dilute solution there is not enough reactant left for the growth of the crystals. As a result, the particles do not grow beyond 12 nm. The MAH process at KOH showed most effective to dehydrate the adsorbed water

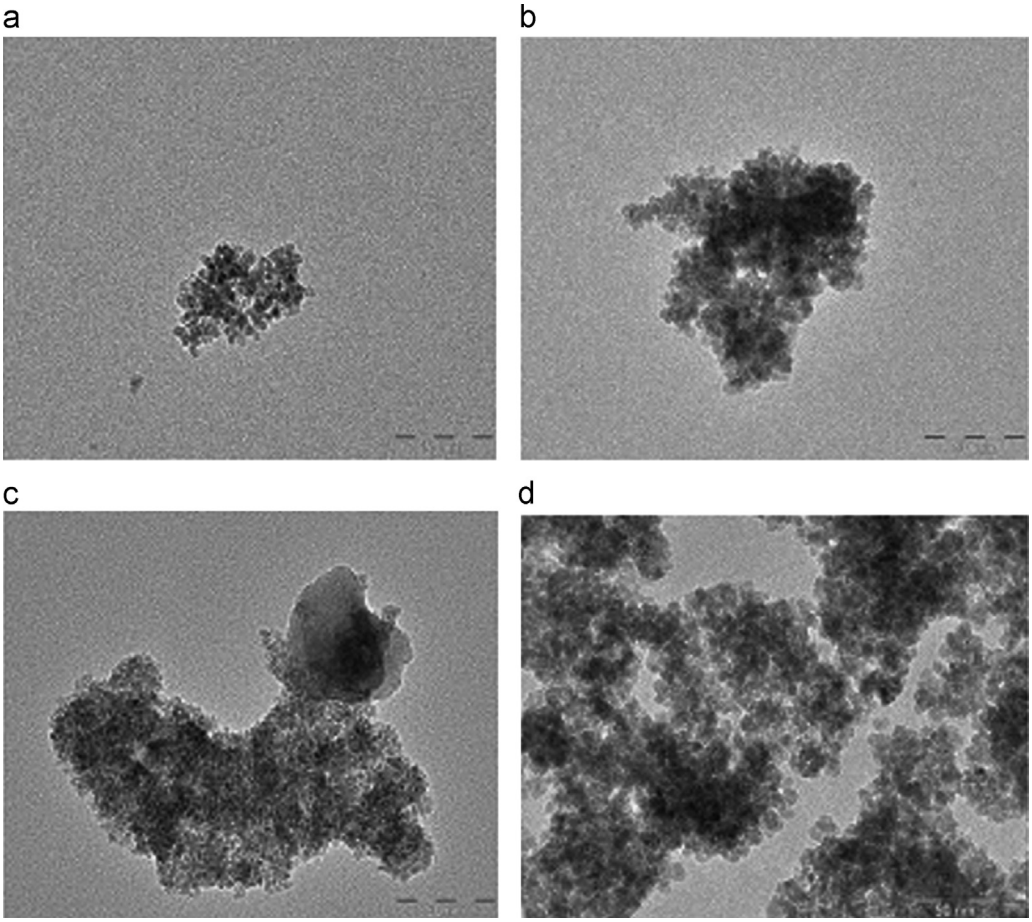

Fig. 4. TEM images of $Ce_{1-3/4x}Pr_xO_2$ nanoparticles synthesized at 100 °C in the MAH method under KOH mineralizer at different contents: (a) 0; (b) 1.6; (c) 5.0 and (d) 10.

and decrease the hydrogen bonding effect leaving a weakly agglomerated nanoparticles of hydrated ceria. Alternatively, if the solution was maintained at basicity, it might be due to crystallization from amorphous gel through a dissolution-precipitation, because solubility of cerium hydroxide is very high in the strong basic solution. Aggregation between the particles decreases and monodispersed particles are observed at higher Pr content. The higher agglomeration degree of undoped CeO_2 is due the Van der Waal's force derived for the –OH ligand precursor which was transformed to CeO_2 after hydrothermal treatment. Moreover, the distribution in size seemed to be homogeneous and the shape appeared rounded. The synthesized CeO_2 nanocrystals were relatively spherical with uniform size distribution. Nanometric and isotropic CeO_2 crystallites obtained in this study are quite different from the previous study, where CeO_2 nanocrystals agglomerated into a cubic shape with the side size of 4.8 nm under hydrothermal conditions [54]. The images taken confirm the formation of nanocrystallites with uniform grain size and the absence of partial sintering or excessive growth of any nanocrystallites.

Fig. 5 shows the PL spectra of CeO_2 nanocrystals synthesized by MAH at 100 °C as Pr content increases of 0, 1.6, 5 and 10, respectively. All the observations can be simply summarized. Whatever the sample, band at 609 nm became more intense as particle size was reduced by hydrothermal treatment. As a consequence these bands may be attributed to bulk energy levels. This is consistent with their attribution to CT transitions between O^{2-} and Ce^{4+} [55]. The band at 459 nm was shifted and became less intense with hydrothermal treatment: the effect was limited due to the particle size. The main difference between the samples under hydrothermal ripening was their crystal growth: very weak for a higher particle size, significant for a lower particle size. As a consequence this band may be attributed to surface specific

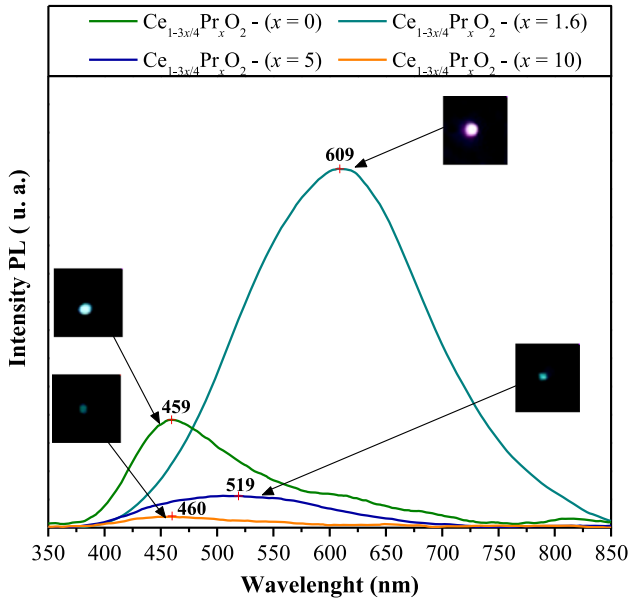

Fig. 5. PL spectra at room temperature of $Ce_{1-3/4x}Pr_xO_2$ nanoparticles synthesized at 100 °C in the MAH method under KOH mineralizer at different contents: (a) 0; (b) 1.6; (c) 5.0 and (d) 10.

defects that disappear during growth under hydrothermal conditions. It is noteworthy that these defects systematically exist in particles obtained by room temperature precipitation, whatever the pH, pressure and particle size are predominant. Interestingly, some cerium oxide particles directly synthesized in hydrothermal conditions did exhibit PL bands at 370 and 414 nm without significant emission at 460 nm [56], confirming that the intense peak at 459 nm was highly dependent from preparation processes. PL emission can be changed due to the presence of a large amount of defects associated to the Pr content which affects the particle size and level of defects. The PL is strongly dependent on the Pr content, due its addition cause a reduction in the defects or disorder of materials. Intensity of PL emission changes with the increase of Pr content, as indicated in Fig. 6. This intensity is likely associated with structural desorganization level, and the charge transfer occurring between cerium, praseodymium and oxygen ions. However, it is very important to note that at this condition no electronic levels of the amorphous $[CeO_8]$ and $[PrO_8]$ clusters included in the wideband gap of the crystalline cluster were evidenced. This conclusion is a good indication that the PL of CeO_2 nanocrystals obtained by the MAH originates from intrinsic defects and charge transfer after a certain degree of structural order. In Fig. 6, it was observed that the PL intensity can be influenced by the processing time in a MAH system. This behavior is not associated to the band-to-band emission process due to the wavelength's energy (2.54 eV) to be small than the E_{gap} of CeO_2 nanocrystals. Probably, the PL of these powders is arising from the contribution of different intermediary energy levels within the band gap. Our results indicate that the CeO_2 nanoparticles processed in MAH are highly crystalline and structurally ordered at long and short range, in agreement with XRD patterns (Fig. 1). Therefore, PL of these powders is not due to effect of distortion in regular hexahedron $[CeO_8]$ clusters at medium-range. As previously described, we believe that the behavior of this physical property is related to the influence of microwave radiation on the $[CeO_8]$ octahedron groups. In this figure, the $1 \times 1 \times 1$ unit cell of CeO_2 crystals with $Fm\bar{3}m$ space was modeled using the Java Structure Viewer Program (Version 1.08 lite for Windows) and VRML-View (Version 3.0 for Windows) [57,58]. We believe that the interaction between microwave radiation and regular hexahedron $[CeO_8]$ clusters results in a rapid heating and leads to a vibration on the charged particles (Fig. 6a). These factors probably result in a distortion process on the regular hexahedron $[CeO_8]$ and $[PrO_8]$ clusters, favoring the formation of intermediary energy levels within the band gap of this material (Fig. 6b–d). These energy levels are composed of oxygen 2*p* states (near the valence band) and praseodymium 5*d* levels (below the conduction band). During the excitation process with 488 nm wavelength, some electrons are promoted from the oxygen 2*p* states to praseodymium 5*d* levels through the absorption of photons ($h\nu$). This mechanism results in the formation of self-trapped excitons (STEs), i.e., trapping of electrons (e^-) by holes (h). The emission process of photons ($h\nu$) occurs when an electron localized in a praseodymium 5*d* levels decays into

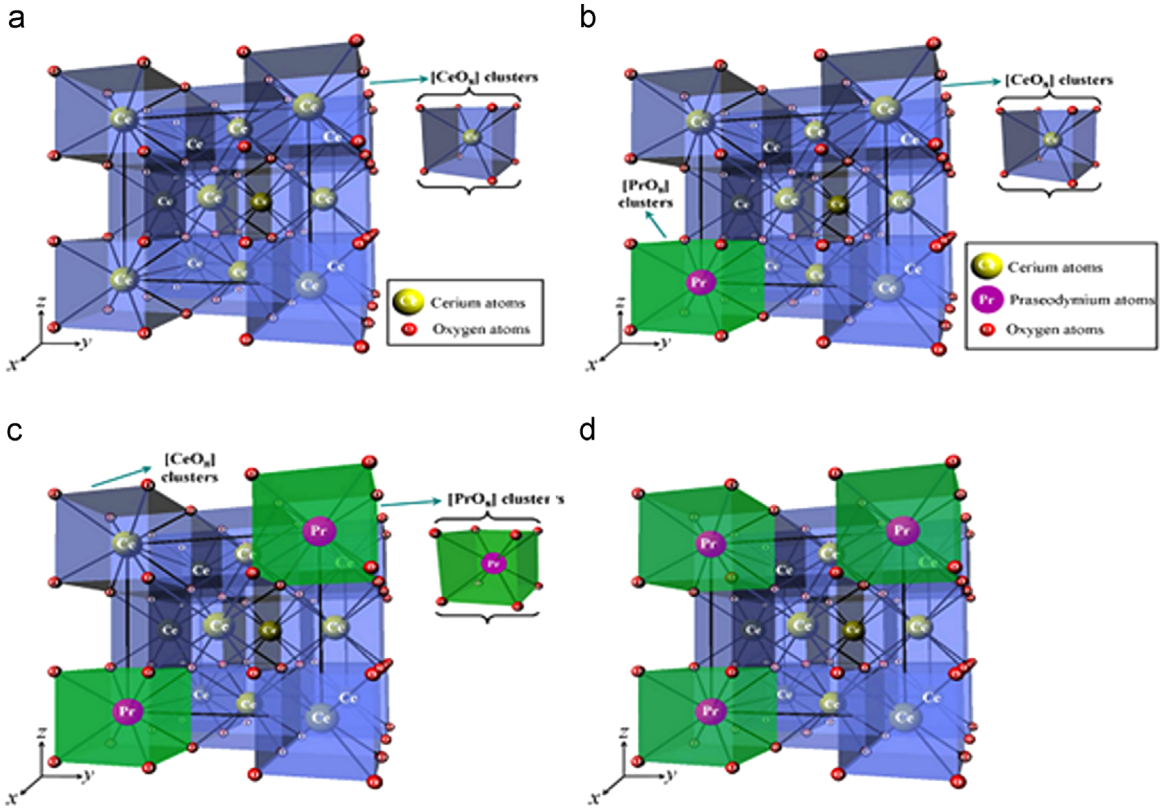

Fig. 6. $1 \times 1 \times 1$ unit cell of $Ce_{1-3/4x}Pr_xO_2$ nanoparticles synthesized at 100 °C in the MAH method under KOH mineralizer at different contents: (a) 0; (b) 1.6; (c) 5.0 and (d) 10 using the Java Structure Viewer Program (Version 1.08 lite for Windows) and VRML-View (Version 3.0 for Windows).

an empty oxygen 2*p* state. Consequently, this mechanism is responsible for the PL emission of CeO_2 nanoparticles. This proposed mechanism based on the distortion regular hexahedron [CeO_8] and [PrO_8] clusters, consequently can be related with the non-linear variations on the PL intensity of CeO_2 nanocrystals with the Pr^{3+} ions content in MAH (Fig. 6). Also, this behavior can be associated with the formation of superficial defects caused by the modifications on the morphology of these powders [59]. These defects are arising from rapid heating, high effective collision rates between the small particles and growth processes during the processing of CeO_2 nanoparticles. However, future investigations will be necessary in order to understand the effect of microwave-radiation on the PL properties.

4. Conclusions

In summary, the MAH method as synthesis method it is possible to obtain, by treating the solution at 100 °C nanometric and crystalline CeO_2 nanocrystals. Raman scattering revealed the first scattering mode which is typical for cubic fluorite structure. UV–vis spectra revealed that as Pr content increases, the optical band gap of the sample initially increases and then decreases because new levels of energy are formed promoting the appearance of intermediate electronic levels in the band gap. TEM analysis has shown that undoped CeO_2 powders obtained displays poor contrast and intense agglomeration amongst extremely fine particles. Aggregation between the particles decreases and monodispersed particles are observed at higher Pr content. The PL emission intensity depends on different types of defects generated by a possible configuration arrangement interconversion in solution during CeO_2 growth. The mechanism responsible for the PL emission of CeO_2 nanoparticles doped with Pr is a consequence of emission process of photons ($h\nu$) when an electron localized in a praseodymium 5*d* levels decays into an empty oxygen 2*p* state. MAH method is important not only for the use of a short treatment time and low temperature but also for the possibility to control the morphological and structural properties. Therefore, the MAH method is undeniably a genuine technique for low temperatures and short times in comparison with the previous methodologies.

Acknowledgments

The financial support of this research project by the Brazilian research funding agencies CNPq and FAPESP is gratefully acknowledged.

References

[1] B.M. Reddy, A. Khan, Y. Yamada, T. Kobayashi, S. Loridant, J.C. Volta, Raman and X-ray photoelectron spectroscopy study of CeO_2-ZrO_2 and V_2O_5/CeO_2-ZrO_2 catalysts, Langmuir 19 (2003) 3025–3030.

[2] P. Bera, A. Gayen, M.S. Hegde, N.P. Lalla, L. Spadaro, F. Frusteri, F. Arena, Promoting effect of CeO_2 in combustion synthesized Pt/CeO_2

catalyst for CO oxidation, Journal of Physical Chemistry B 107 (2003) 6122–6130.
[3] G. Jacobs, L. Williams, U. Graham, D. Sparks, B.H. Davis, Low-temperature water-gas shift: In-situ DRIFTS – reaction study of a Pt/CeO_2 catalyst for fuel cell reformer applications, Journal of Physical Chemistry B 107 (2003) 10398–10404.
[4] R.X. Li, S. Yabe, M. Yamashita, S. Momose, S. Yoshida, S. Yin, T. Sato, Synthesis and UV-shielding properties of ZnO- and CaO-doped CeO_2 via soft solution chemical process, Solid State Ionics 151 (2002) 235–241.
[5] K. Sohlberg, S.T Pantelides, S.J. Pennycook, Interactions of hydrogen with CeO_2, Journal of the American Chemical Society 123 (2001) 6609–6611.
[6] P. Jasinski, T. Suzuki, H.U. Anderson, Nanocrystalline undoped ceria oxygen sensor, Sensors and Actuators B Chemical 95 (2003) 73–77.
[7] F. Goubin, X. Rocquefelte, M.H Whangbo, Y. Montardi, R. Brec, S. Jobic, Experimental and theoretical characterization of the optical properties of CeO_2, $SrCeO_3$, and Sr_2CeO_4 containing Ce^{4+} (f(0)) ions, Chemistry of Materials 16 (2004) 662–669.
[8] D.G Shchukin, R.A Caruso, Template synthesis and photocatalytic properties of porous metal oxide spheres formed by nanoparticle infiltration, Chemistry of Materials 16 (2004) 2287–2292.
[9] B. Djuricic, S. Pickering, Nanostructured cerium oxide: Preparation and properties of weakly-agglomerated powders, Journal of the European Ceramic Society 19 (1999) 1925–1934.
[10] S. Dikmen, P Shuk, M. Greenblatt, H. Gocmez, Hydrothermal synthesis and properties of $Ce_{1-x}Gd_{xO_2}$-delta solid solutions, Solid State Sciences 4 (2002) 585–590.
[11] S.W Zha, C.R Xia, G.Y Meng, Effect of Gd (Sm) doping on properties of ceria electrolyte for solid oxide fuel cells, Journal of Power Sources 115 (2003) 44–48.
[12] Y.R. Wang, T. Mori, J.G Li, T. Ikegami, Low-temperature synthesis of praseodymium-doped ceria nanopowders, Journal of the American Ceramic Society 85 (2002) 3105–3107.
[13] J.G. Li, T. Ikegami, Y.R Wang, T. Mori, 10-mol%-Gd_2O_3-doped CeO_2 solid solutions via carbonate coprecipitation: a comparative study, Journal of the American Ceramic Society 86 (2003) 915–921.
[14] M.J. Godinho, R.F. Goncalves, L.P.S. Santos, J.A. Varela, E. Longo, E.R. Leite, Room temperature co-precipitation of nanocrystalline CeO_2 and $Ce_{0.8}Gd_{0.2}O_{1.9}$-delta powder, Materials Letters 61 (2007) 1904–1907.
[15] R.A. Rocha, E.N.S. Muccillo, Preparation and characterization of $Ce_{0.8}Gd_{0.2}O_{1.9}$ solid electrolyte by polymeric precursor techniques, Advanced Powder Technology Iii 416 (2003) 711–717.
[16] S. Wang, K. Maeda, Direct formation of crystalline gadolinium-doped ceria powder via polymerized precursor solution, Journal of the American Ceramic Society 85 (2002) 1750–1752.
[17] F. Bondioli, A.B. Corradi, T. Manfredini, G. Leonelli, R. Bertoncello, Nonconventional synthesis of praseodymium-doped ceria by flux method, Chemistry of Materials 12 (2000) 324–330.
[18] S. Maensiri, C. Masingboon, P. Laokul, W. Jareonboon, V. Promarak, P. Anderson, S. Seraphin, Egg white synthesis and photoluminescence of platelike clusters of CeO_2 nanoparticles, Crystal Growth and Design 7 (2007) 950–955.
[19] A. Morshed, M. Moussa, S. Bedair, R. Leonard, S. Liu, N. El-masry, Violet/blue emission from epitaxial cerium oxide films on silicon substrates, Applied Physics Letters 70 (1997) 1647–1649.
[20] H.M. Yang, C.H. Huang, A.D. Tang, X.C. Zhang, W.G. Yang, Microwave-assisted synthesis of ceria nanoparticles, Materials Research Bulletin 40 (2005) 1690–1695.
[21] M. Natile, G.M. Boccaletti, A. Glisenti, Properties and reactivity of nanostructured CeO_2 powders: Comparison among two synthesis procedures, Chemistry of Materials 17 (2005) 6272–6286.
[22] J.S. Lee, S.C. Choi, Crystallization behavior of nano-ceria powders by hydrothennal synthesis using a mixture of H_2O_2 and NH_4OH, Materials Letters 58 (2004) 390–393.
[23] S. Komarneni, R. Roy, Q.H. Li, Microwave-hydrothermal synthesis of ceramic powders, Materials Research Bulletin 27 (1992) 1393–1405.
[24] S. Komarneni, Q. Li, K.M. Stefansson, R. Roy, Microwave-hydrothermal processing for synthesis of electroceramic powders, Journal of Materials Research 8 (1993) 3176–3183.
[25] S. Komarneni, Q.H Li, R. Roy, Microwave-hydrothermal processing for synthesis of layered and network phosphates, Journal of Materials Chemistry 4 (1994) 1903–1906.
[26] S. Komarneni, R. Pidugu, Q.H. Li, R. Roy, Microwave-hydrothermal processing of metal powders, Journal of Materials Research 10 (1995) 1687–1692.
[27] F. Gao, Q. Lu, S. Komarneni, Fast synthesis of cerium oxide nanoparticles and nanorods, Journal of Nanoscience and Nanotechnology 6 (2006) 3812–3819.
[28] A.B. Corradi, F.B. Bondioli, A.M. Ferrari, T. Manfredini, Synthesis and characterization of nanosized ceria powders by microwave-hydrothermal method, Materials Research Bulletin 41 (2006) 38–44.
[29] T.N. Glasnov, C.O. Kappe, The microwave-to-flow paradigm: translating high-temperature batch microwave chemistry to scalable continuous-flow processes, Chemistry – A European Journal 17 (2011) 11956–11968.
[30] A. De la Hoz, A. Díaz-Ortiz, A. Moreno, Microwaves in organic synthesis. Thermal and non-thermal microwave effects, Chemical Society Reviews 34 (2005) 164–178.
[31] C.O. Kappe, Controlled microwave heating in modern organic synthesis, Angewandte Chemie International Edition 43 (2004) 6250–6284.
[32] T.L.C. Martins, T.C.C. França, C. Teodorico, T.C. Ramalho, J.D.F. Villar, Synthesis of guanylhydrazones under microwave irradiation, Synthetic Communications 34 (2004) 3891–3899.
[33] I. Bilecka, M. Kubli, E. Amstad, M. Niederberger, Simultaneous formation of ferrite nanocrystals and deposition of thin films via a microwave-assisted nonaqueous sol–gel process, Journal of Sol–Gel Science and Technology 57 (2011) 313–322.
[34] M. Estruga, C. Domingo, J.A Ayllon, Microwave radiation as heating method in the synthesis of titanium dioxide nanoparticles from hexafluorotitanate-organic salts, Materials Research Bulletin 45 (2010) 1224–1229.
[35] V. Abdelsayed, A. Aljarash, M.S. El-Shall, Z.A. Al Othman, A.H. Alghamdi, Microwave synthesis of bimetallic nanoalloys and CO oxidation on ceria-supported nanoalloys, Chemistry of Materials 21 (2009) 2825–2834.
[36] M. Baghbanzadeh, S.D. Skapin, Z.C. Orel, C.O Kappe, A critical assessment of the specific role of microwave irradiation in the synthesis of ZnO micro- and nanostructured materials, Chemistry – A European Journal 18 (2012) 5724–5731.
[38] S. Saremi-Yarahmadi, B. Vaidhyanatha, K.G. Upul Wijayantha, Microwave-assisted low temperature fabrication of nanostructured α-Fe_2O_3 electrodes for solar-driven hydrogen generation, International Journal of Hydrogen Energy 35 (2010) 10155–10165.
[39] R.G. Deshmukh, S.S. Badadhe, I.S. Mulla, Microwave-assisted synthesis and humidity sensing of nanostructured α-Fe_2O_3 44 (2009) 1179–1182Materials Research Bulletin 44 (2009) 1179–1182.
[40] I. Bilecka, M. Niederberger, Microwave chemistry for inorganic nanomaterials synthesis, Nanoscale 2 (2010) 1358–1374.
[41] M. Baghbanzadeh, L. Carbone, P.D. Cozzoli, C.O. Kappe, Microwave-assisted synthesis of colloidal inorganic nanocrystals, Angewandte Chemie International Edition 50 (2011) 11312–11359.
[42] L.F. Silva, W. Waldir Avansi, M.L. Moreira, E. Longo, V.R. Mastelaro, Novel $SrTi_{1-x}Fe_xO_3$ nanocubes synthesized by microwave-assisted hydrothermal method, CrystEngComm 14 (2012) 4068–4073.
[43] M.L. Moreira, A. Juan, V.R. Mastelaro, J.A. Varela, E. Longo, On the reversed crystal growth of $BaZrO_3$ decaoctahedron: shape evolution and mechanism, CrystEngComm 13 (2011) 5818–5824.
[44] L.R. Macario, M.L. Moreira, A. Juan, E. Longo, An efficient microwave-assisted hydrothermal synthesis of $BaZrO_3$ microcrystals: growth mechanism and photoluminescence emissions, CrystEngComm 12 (2010) 3612–3619.
[45] D.-E. Zhang, X.-M. Ni, H.-G. Zheng, X.-J. Zhang, J.-M. Song, Fabrication of rod-like CeO_2: Characterization, optical and electrochemical properties, Solid State Sciences 8 (2006) 1290–1293.
[46] S. Yu, H. Cölfen, A. Fischer, High quality CeO_2 nanocrystals stabilized by a double hydrophilic block copolymer, Colloids and Surfaces 243 (2004) 49–52.
[47] A Tok, S. Du, F. Boey, W. Chong, Hydrothermal synthesis and characterization of rare earth doped ceria nanoparticles, Materials Science and Engineering: A 466 (1) (2007) 223–229, http://dx.doi.org/10.1016/j.msea.2007.02.083.

[48] H. Li, G. Lu, Y. Wang, Y. Guo, Synthesis of flower-like La or Pr-doped mesoporous ceria microspheres and their catalytic activities for methane combustion, Catalysis Communications 11 (11) (2010) 946–950, http://dx.doi.org/10.1016/j.catcom.2010.04.006.

[49] F. Gao, G. Li, J. Zhang, F. Qin, Z. Yao, Z. Liu, Z. Wang, L. Lin, Growth and photoluminescence of epitaxial CeO_2 film on Si (111) substrate, Chinese Physics Letters 18 (2001) 443–444.

[50] Y Takasu, T Sugino, Y. Matsuda, Electrical conductivityof praseodymia doped ceria, Journal of Applied Electrochemistry 14 (1) (1984) 79–81, http://dx.doi.org/10.1007/BF00611261.

[51] B. Djuricic, S. Pickering, Silica-supported Au nanoparticles decorated by CeO_2: formation, morphology, and CO oxidation activity, Journal of the European Ceramic Society 19 (1999) 1925–1934.

[52] H.R. Tan, J.P.Y. Tan, C. Boothroyd, T.W. Hansen, Y.L. Foo, M.J. Lin, Experimental evidence for self-assembly of CeO_2 particles in solution: formation of single-crystalline porous CeO_2 nanocrystals, Journal of Physical Chemistry C 116 (2012) 242–247.

[53] P. Kubelka, F. Munk, Ein Beitrag zur Optik der Farbanstriche, Zeits. F. Techn. Physik. 12 (1931) 593–601.

[54] G.J. Wilson, A.S. Matijasevich, D.R.G. Mitchell, J.C. Schulz, G.D. Will, Modification of TiO_2 for enhanced surface properties: finite Ostwald ripening by a microwave hydrothermal process, Langmuir 22 (2006) 2016–2027.

[55] Y.W. Zhang, S. Rui, C.S. Liao, C.H. Yan, Fe doped CeO_2 nanoparticles, Journal of Physical Chemistry B 107 (2003) 10159–10163.

[56] M. Hirano, M. Inagaki, Preparation of monodispersed cerium (IV) oxide particles by thermal hydrolysis: influence of the presence of urea and Gd doping on their morphology and growth, Journal of Materials Chemistry 10 (2000) 473–477.

[57] J.R. McBride, K.C. Hass, B.D. Poindexter, W.H. Weber, Template preparation of nanoscale $Ce_xFe_{1-x}O_2$ solid solutions, Journal of Applied Physics 76 (1994) 2435–2441.

[58] P. Fornasiero, G. Balducci, R. DiMonte, J. Kaspar, V. Sergo, G. Gubitosa, Modification of the redox behaviour of CeO_2 induced by structural doping with ZrO_2, Journal of Catalysis 164 (1996) 83–173.

[59] M. Pineda, J.L.G. Fierro, J.M. Palacios, C. Cilleruelo, E. Garcia, J. V. Ibarra, Characterization of zincoxide and zinc ferrite doped with Ti or Cu as sorbents for hotgasdesulphurization, Applied Surface Science 119 (1997) 1–10.